

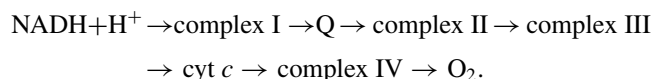
**Long-range donor-acceptor electron transport mediated by  $\alpha$  helices**L. S. Brizhik <sup>\*</sup>*Bogolyubov Institute for Theoretical Physics, National Academy of Sciences of Ukraine, 03143 Kyiv, Ukraine*J. Luo <sup>†</sup>*School of Mathematics, University of Birmingham, Birmingham B15 2TT, United Kingdom*B. M. A. G. Piette <sup>‡</sup> and W. J. Zakrzewski <sup>§</sup>*Department of Mathematical Sciences, University of Durham, Durham DH1 3LE, United Kingdom*

(Received 28 August 2019; published 19 December 2019)

We study the long-range electron and energy transfer mediated by a polaron on an  $\alpha$ -helix polypeptide chain coupled to donor and acceptor molecules at opposite ends of the chain. We show that for specific parameters of the system, an electron initially located on the donor can tunnel onto the  $\alpha$  helix, forming a polaron, which then travels to the other extremity of the polypeptide chain, where it is captured by the acceptor. We consider three families of couplings between the donor, the acceptor, and the chain and show that one of them can lead to a 90% efficiency of the electron transport from donor to acceptor. We also show that this process remains stable at physiological temperatures in the presence of thermal fluctuations in the system.

DOI: [10.1103/PhysRevE.100.062205](https://doi.org/10.1103/PhysRevE.100.062205)**I. INTRODUCTION**

The mechanisms behind the highly efficient long-range electron transfer (ET) in redox reactions accompanying photosynthesis and cellular respiration have been intensively discussed over several decades [1,2]. This transfer takes place at macroscopic distances along the so-called electron transport chain in Krebs cycles in membranes of chloroplasts, mitochondria, or cells and occurs at physiological temperatures. Conventional mechanisms such as tunneling and the Förster and Dexter mechanisms [3–5] cannot provide such long-range ET even at zero temperature, let alone 300 K. Nevertheless, it should be noted that the very structure of the ET chain can facilitate these processes. An ET chain consists of a spatially separated sequence of biological molecular complexes (peptides, enzymes, etc.), along which the sequential transport of electrons takes place via redox processes, so that every site in this chain plays the role of an acceptor for the left neighbor and a donor for the right one along the chain (see, e.g., [6]). The electron transport chain in mitochondria can be schematically represented as the following sequence:



Here  $\text{NADH} + \text{H}^+$  is nicotinamide adenine dinucleotide, which serves as the substrate; complex I is NADH coenzyme Q reductase; Q is ubiquinone coenzyme; complex II is succinate dehydrogenase; complex III is cytochrome  $bc_1$ ; cyt  $c$  is cytochrome  $c$ ; complex IV is cytochrome  $c$  oxidase; and  $\text{O}_2$  is

molecular oxygen. Another example of the electron transport chain can be found in [7].

In each elementary process, at the onset, there is a release of four electrons at the substrate, which then are carried along the chain with the reduction of molecular oxygen and hydrogen ions to a water molecule at the final stage of the process. This transport of electrons is so exceptionally efficient that only a tiny percentage of electrons leak out to reduce oxygen. The complexes in the ET chain can be conventionally divided into two groups: heavy and light ones. In particular, in ET chains, elements such as ubiquinone or cytochrome  $cyt-c$  have relatively small molecular weight, which leads to their high mobility. They can move outside the mitochondrial membrane, carrying electrons from a heavy donor to a heavy acceptor via a linear, e.g., the Förster mechanism [3,5]. Some other complexes in the electron transport chain, such as NADH-ubiquinone oxidoreductase, flavoproteids, cytochrome  $c$ -oxidase,  $cyt\ aa_3$ , and cytochrome  $cyt\ bc_1$ , are proteins with higher molecular weight of up to several hundreds of kilodaltons. Conventional linear mechanisms cannot provide coherent transport of electrons across these heavy enzymes, either as a whole or internally between cofactors separated by macroscopic distances, for instance, porphyrins, metal clusters, etc., that are separated by macroscopic distance. Nevertheless, their regular crystal-like structure can facilitate ET, as is discussed below. For instance, inside some large enzymes like NADH ubiquinone oxidoreductase there can be several long pathways for electron transport [2], where one can identify the  $\alpha$ -helical part of the enzyme between the donor and the acceptor.

A significant part of heavy macromolecules is in the  $\alpha$ -helical conformation, whose regular structure results in the formation of electron bands in their energy spectrum. The  $\alpha$ -helical structure is stabilized by relatively weak hydrogen bonds resulting in strong electron-lattice interactions, and

<sup>\*</sup>brizhik@bitp.kiev.ua<sup>†</sup>j.luo.5@bham.ac.uk<sup>‡</sup>B.M.A.G.Piette@durham.ac.uk<sup>§</sup>w.j.zakrzewski@durham.ac.uk

thus in the polaron effect. An  $\alpha$ -helical segment of a protein contains three almost-parallel polypeptide strands bound by hydrogen bonds along the strands, with weak interactions between these strands. An isolated strand is described by the Fröhlich Hamiltonian, and this description leads to a system of coupled nonlinear equations for the electron wave function and lattice variables and admits soliton solutions. The possibility of self-trapping of electrons in an isolated one-dimensional molecular chain, like a polypeptide strand, was first shown in [8] (see also [9,10]) and later it was also demonstrated in helical systems [11–13]. The soliton solutions of these models are particular cases of a large polaron. Such a polaron can be described as a crossover between an almost-free electron and small polaron states depending on the strength of the exchange interaction energy, the electron-lattice coupling constant, the number of phonon modes, their type, and the corresponding Debye energies [14]. The soliton properties depend on the parameters of the system. Moreover, the helical structure of proteins was shown to lead to the existence of several types of soliton solutions of the model with different properties and symmetries [13]. In such soliton states electrons can propagate along macromolecules almost without any loss of energy.

The results mentioned above have been obtained for isolated strands or helices, while in reality, the electron transport occurs in the donor-bridge-acceptor system, as is the case for the ET chain in the Krebs cycles. The simple case when the bridge is modeled as a polypeptide strand was studied in [15]. It was shown there that the long-range ET can be provided by the soliton mechanism within a wide range of parameter values of the donor, acceptor, and polypeptide strands.

In the present paper we study the possibility of a coherent long-range electron transport in the donor- $\alpha$ -helix-acceptor system. As one can expect, the formation of the soliton on the  $\alpha$  helix depends on the helix-donor and helix-acceptor couplings, as well as on the parameters of the system under study (see, e.g., [15–17]), and we can find conditions which lead to the formation of a soliton on the helix.

There are two other aspects of the model developed in the present paper. The first one is related to the fact that the functioning of the ET chain is tightly connected with the production of adenosine triphosphate (ATP): In most organisms the majority of ATP is generated in ET chains (see, e.g., [18]). The energy of the hydrolysis of ATP into ADP is the basic unit of energy used in biological systems, in particular in muscles to produce mechanical work and to establish electrochemical gradients across membranes, in biosynthetic processes, and in many other physiological and biochemical processes necessary to maintain life. The amount of energy released by ATP hydrolysis is approximately 0.43 eV, which is only 20 times the thermal energy at physiological temperatures and is not enough for an electronic excitation. It is sufficient to excite some vibrations, such as an amide I vibration, an excitation which requires an energy of 0.21 eV. Amide I is mainly (up to 80%) the stretching vibration of a double C=O bond of the peptide group, which has a relatively large dipole moment 0.3 D oriented along the  $\alpha$ -helix axis. This excitation is registered in optical spectra of polypeptide molecules, its wavelength being  $1650\text{ cm}^{-1}$ , and, according to [19], the ATP hydrolysis energy is transferred along protein macromolecules in the

form of amide I vibration. (For more details see [9,10,20–22] or the more recent [23,24].)

As has been shown by Davydov, the amide I vibration can be self-trapped in a macromolecule into a soliton state and carried along it to the place where it is utilized for biochemical or mechanical needs [9,10]. This process, from a mathematical point of view, is described formally by the same system of equations as the ET. Therefore, the results obtained here are equally valid for such energy transfer processes.

The second aspect of the model is related to the potential importance of our results for micro- and nanoelectronics where conjugated donor-acceptor copolymer semiconductors with intramolecular charge transfer on large distances are widely used. A large number of such systems have been recently synthesized. They include donor-acceptor pairs mediated by salt bridges [25], thienopyrazine-based copolymers [26], and some others [27–29]. Donor-bridge-acceptor systems with efficient ET play an important role in electronic applications [30–33]: They can be used in photovoltaic cells [29,34–36], light-emitting diodes [37–40], and field-effect transistors [41–44], in particular thin-film organic field-effect transistors [45]. Proteins and synthetic macromolecules have great technological potential; one example is the improvement of efficiency and UV photostability of planar perovskite solar cells using amino-functionalized conjugated polymers as ET materials [27,29].

Recent novel applications in bioelectronics such as organic photovoltaics and fuel cell technology are based on metalorganic frameworks or structures that are complexes of electroconducting compounds or substrates and polypeptides (see, e.g., [46–48] and references therein). It has been shown that both the peptide composition and structure can affect the efficiency of electron transport across peptides [47]. Moreover, long-range conductivity and enhanced solid-state electron transport in proteins and peptide bioelectronic materials have been proven experimentally [49,50]. The effectiveness of electron transport processes in living systems is already used in novel electronic devices, e.g., in *Shewanella Oneidensis* MR-1 cells, based on multi-heme cytochrome-mediated redox conduction [51], or in synthesized supramolecular charge-transfer nanostructures based on peptides [52], synthetic biological protein nanowires with high conductivity [53], self-assembled peptide nanotubes used as electronic materials [54], and many others. We quote Ref. [49]: “The ability of such natural and synthetic protein and peptide materials to conduct electricity over micrometer to centimeter length scales, however, is not readily understood from a conventional view of their amino acid building blocks. Distinct in structure and properties from solid-state inorganic and synthetic organic metals and semiconductors, supramolecular conductive proteins and peptides require careful theoretical treatment. . . .” This is one of the factors which have motivated our interest in the problems discussed in the present paper and we hope that our study will shed some light on this problem.

In the next section we derive a model of the  $\alpha$  helix coupled to a donor molecule and an acceptor molecule. This model is a combination of the models derived in [13,15]. We then perform a parameter scaling to make all the parameters

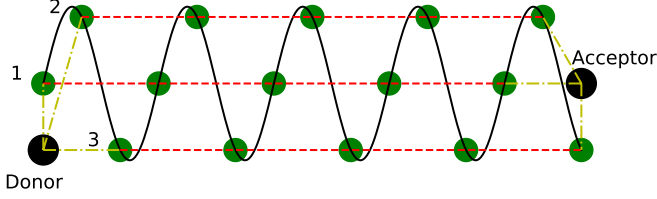


FIG. 1. Model of the  $\alpha$  helix with a donor and an acceptor. The solid line represents the helix backbone formed by chemical bonds, the dashed lines represent the hydrogen bonds that are links along the strands, and the dash-dotted lines represent the links between the donor or acceptor and the different strands. The numbers 1, 2, and 3 label the three strands.

dimensionless and derive the equations in such units. After selecting the parameters that best describe the  $\alpha$ -helical protein, we compute the profile of a static self-trapped electron state (solitonlike or, in other words, large polaron state, which for simplicity we call from now on a polaron) by solving the model equations numerically. We then study various configurations where the electron density has been set to 1 on the donor and 0 elsewhere and let the system evolve. We do this for three different types of couplings between the donor and acceptor to the  $\alpha$  helix and we determine numerically the donor and acceptor coupling parameters that lead to the best transfers of the electron. We end the paper by describing the solutions we have found and draw some conclusions.

## II. MODEL OF THE DONOR- $\alpha$ -HELIX-ACCEPTOR SYSTEM

We consider a polypeptide chain in an  $\alpha$ -helical configuration made out of  $N$  peptide groups (PGs), with a donor molecule attached to one end and an acceptor molecule attached to the other end. The peptide chain forms a helical structure in which each molecule is coupled by chemical bonds to its neighbors along the chain as well as to the PG three sites away from it by hydrogen bonds. With this three-step coupling, the  $\alpha$  helix can also be seen as three parallel chains [55], which we refer to as strands in what follows. This model is depicted in Fig. 1.

We label the PGs with the index  $n$  along the polypeptide chain and use  $n = 0$  for the donor and  $n = N + 1$  for the acceptor. This means that PGs with an index difference which is a multiple of 3 belong to the same strand of the  $\alpha$  helix.

The donor and the acceptor can, *a priori*, be coupled, respectively, to the first three and the last three peptides, i.e., with the nodes  $n = 1, 2, 3$  and  $N = N - 2, N - 1, N$ . In our study, we will consider three different types of couplings, but for now we assume that all the coupling parameters are different.

The Hamiltonian of the system is given by

$$\mathcal{H} = \mathcal{H}_e + \mathcal{H}_p + \mathcal{H}_{\text{int}}, \quad (1)$$

where  $\mathcal{H}_e$ ,  $\mathcal{H}_p$ , and  $\mathcal{H}_{\text{int}}$  are, respectively, the phonon, electron, and interaction Hamiltonians given by

$$\begin{aligned} \mathcal{H}_e = & \bar{E}_d |\Psi_0|^2 + \bar{E}_a |\Psi_{N+1}|^2 + \bar{E}_0 \sum_{n=1}^N |\Psi_n|^2 - \bar{J} \sum_{n=1}^{N-3} (\Psi_n \Psi_{n+3}^* + \Psi_{n+3} \Psi_n^*) + \bar{L} \sum_{n=1}^{N-1} (\Psi_n \Psi_{n+1}^* + \Psi_{n+1} \Psi_n^*) \\ & - \sum_{\ell=1}^3 \bar{D}_{d,\ell} (\Psi_0 \Psi_\ell^* + \Psi_\ell \Psi_0^*) - \sum_{\ell=1}^3 \bar{D}_{a,\ell} (\Psi_{N+1} \Psi_{N-3+\ell}^* + \Psi_{N-3+\ell} \Psi_{N+1}^*), \end{aligned} \quad (2)$$

$$\mathcal{H}_p = \frac{1}{2} \left[ \frac{P_d^2}{M_d} + \frac{P_a^2}{M_a} \right] + \frac{1}{2} \sum_{\ell=1}^3 [\bar{W}_{d,\ell} (U_0 - U_\ell)^2 + \bar{W}_{a,\ell} (U_{N+1} - U_{N-3+\ell})^2] + \frac{1}{2} \sum_{n=1}^N \frac{P_n^2}{M} + \frac{1}{2} \sum_{n=1}^{N-3} \bar{W} (U_{n+3} - U_n)^2, \quad (3)$$

$$\begin{aligned} \mathcal{H}_{\text{int}} = & |\Psi_0|^2 \sum_{\ell=1}^3 \bar{\chi}_{d,\ell} (U_\ell - U_0) + |\Psi_{N+1}|^2 \sum_{\ell=1}^3 \bar{\chi}_{a,\ell} (U_{N+1} - U_{N-3+\ell}) + \sum_{\ell=1}^3 |\Psi_\ell|^2 [\bar{\chi}_{d,\ell} (U_\ell - U_0) + \bar{\chi} (U_{\ell+3} - U_\ell)] \\ & + \sum_{\ell=1}^3 |\Psi_{N-3+\ell}|^2 [\bar{\chi}_{a,\ell} (U_{N+1} - U_{N-3+\ell}) + \bar{\chi} (U_{N-3+\ell} - U_{N-6+\ell})] + \bar{\chi} \sum_{n=4}^{N-3} |\Psi_n|^2 (U_{n+3} - U_{n-3}). \end{aligned} \quad (4)$$

In these expressions,  $\bar{E}_0$  describes the on-site electron energy,  $\bar{J}$  the resonance integral along the strands,  $\bar{L}$  the resonance integral along the helix,  $M$  the mass of the unit cell,  $\bar{\chi}$  the electron-lattice coupling, and  $\bar{W}$  the elasticity of the bond along the strands. The constants with subscript  $d$  or  $a$  refer to parameters of the donor and the acceptor, respectively.

The functions  $\Psi_n$  describe the electron wave function (and so  $|\Psi_n|^2$  describes the electron probability of being at the site  $n$ ) and  $U_n$  describe the displacement of molecule  $n$  along the strands;  $P_n$  are the canonically conjugated momenta of  $U_n$ . Of course, the electron wave function satisfies the normalization

condition

$$\sum_{n=0}^{N+1} |\Psi_n|^2 = 1, \quad (5)$$

where, following our convention,  $\Psi_0 = \Psi_d$  and  $\Psi_{N+1} = \Psi_a$ .

Our model is meant to describe the case in which the principal chain can be sufficiently well approximated by one phonon band corresponding to an acoustical phonon mode which describes the longitudinal displacements of the unit cells from their positions of equilibrium along the helix's

strands. The electron-lattice interaction Hamiltonian induces a dependence of the electron Hamiltonian on the lattice distortions. We also assume here that the dependence of the on-site electron energy on the lattice distortion is much stronger than that of the intersite electron interaction energy.

The model we present here is a combination of the polaron model of the  $\alpha$  helix which was described in detail in [13] and of the donor-acceptor model described in [15]. The first model describes polarons on an  $\alpha$  helix, instead of using the traditional single chain, proposed by Davydov [9,10], which corresponds to what we call a strand in this paper. In fact, it was shown in [13] that the polaron is spread over the three strands, hence the relevance of using a more realistic helical model. The paper in [15] describes a model of the transfer

of an electron from a donor molecule to an acceptor one via the coherent propagation of a polaron along a simple chain (a single strand in the present model). The model we describe here is a combination of these two models in which the donor and the acceptor are coupled to a proper  $\alpha$  helix instead of to a single strand.

### III. PARAMETER SCALING

To facilitate the analysis of the model solutions, it is convenient to scale the parameters so that they become dimensionless. Thus, following [13], we perform the following scalings:

$$\begin{aligned}
 d &= 10^{-11} \text{ m}, & u_n &= \frac{U_n}{d}, & \tau &= tv, \\
 E_0 &= \frac{\bar{E}_0}{\hbar v}, & E_d &= \frac{\bar{E}_d}{\hbar v}, & E_a &= \frac{\bar{E}_a}{\hbar v}, \\
 J &= \frac{\bar{J}}{\hbar v}, & D_a &= \frac{\bar{D}_a}{\hbar v}, & D_d &= \frac{\bar{D}_d}{\hbar v}, \\
 W &= \frac{\bar{W}}{v^2 M}, & W_{d,\ell} &= \frac{\bar{W}_{d,\ell}}{v^2 M}, & W_{a,\ell} &= \frac{\bar{W}_{a,\ell}}{v^2 M}, \\
 \chi &= \frac{d\bar{\chi}}{\hbar v}, & \chi_{d,\ell} &= \frac{d\bar{\chi}_{d,\ell}}{\hbar v}, & \chi_{a,\ell} &= \frac{d\bar{\chi}_{a,\ell}}{\hbar v}, \\
 L &= \frac{\bar{L}}{\hbar v}, & K_d &= \frac{M}{M_d}, & K_a &= \frac{M}{M_a}.
 \end{aligned} \tag{6}$$

As a result, the Hamiltonian takes the form  $\mathcal{H}_p = Mv^2 d^2 H_p$ ,  $\mathcal{H}_e = \hbar v H_e$ , and  $\mathcal{H}_{\text{int}} = \hbar v H_{\text{int}}$ , where the dimensionless terms are

$$\begin{aligned}
 H_e &= E_d |\Psi_0|^2 + E_a |\Psi_{N+1}|^2 + E_0 \sum_{n=1}^N |\Psi_n|^2 - J \sum_{n=1}^{N-3} (\Psi_n \Psi_{n+3}^* + \Psi_{n+3} \Psi_n^*) + L \sum_{n=1}^{N-1} (\Psi_n \Psi_{n+1}^* + \Psi_{n+1} \Psi_n^*) \\
 &\quad - \sum_{\ell=1}^3 D_{d,\ell} (\Psi_0 \Psi_\ell^* + \Psi_\ell \Psi_0^*) - \sum_{\ell=1}^3 D_{a,\ell} (\Psi_{N+1} \Psi_{N-3+\ell}^* + \Psi_{N-3+\ell} \Psi_{N+1}^*),
 \end{aligned} \tag{7}$$

$$\begin{aligned}
 H_p &= \frac{1}{2} \left[ \frac{1}{K_d} \left( \frac{du_0}{dt} \right)^2 + \frac{1}{K_a} \left( \frac{du_{N+1}}{dt} \right)^2 \right] + \frac{1}{2} \sum_{\ell=1}^3 [W_{d,\ell} (u_0 - u_\ell)^2 + W_{a,\ell} (u_{N+1} - u_{N-3+\ell})^2] \\
 &\quad + \frac{1}{2} \sum_{n=1}^N \left( \frac{du_n}{dt} \right)^2 + \frac{1}{2} \sum_{n=1}^{N-3} W (u_{n+3} - u_n)^2,
 \end{aligned} \tag{8}$$

$$\begin{aligned}
 H_{\text{int}} &= |\Psi_0|^2 \sum_{\ell=1}^3 \chi_{d,\ell} (U_\ell - U_0) + |\Psi_{N+1}|^2 \sum_{\ell=1}^3 \chi_{a,\ell} (U_{N+1} - U_{N-3+\ell}) + \sum_{\ell=1}^3 |\Psi_\ell|^2 [\chi_{d,\ell} (U_\ell - U_0) + \chi (U_{\ell+3} - U_\ell)] \\
 &\quad + \sum_{\ell=1}^3 |\Psi_{N-3+\ell}|^2 [\chi_{a,\ell} (U_{N+1} - U_{N-3+\ell}) + \chi (U_{N-3+\ell} - U_{N-6+\ell})] + \chi \sum_{n=4}^{N-3} |\Psi_n|^2 (U_{n+3} - U_{n-3}).
 \end{aligned} \tag{9}$$

We must thus have  $Mv^2 d^2 = \hbar v$  and so  $v = \hbar/Md^2$ . With  $M = 1.9112 \times 10^{-25}$  kg [15], as  $\hbar = 1.054 \times 10^{-34}$  Js, we have  $v = 5.51 \times 10^{12}$  s $^{-1}$ .

Before deriving the dimensionless equations it is also convenient to multiply the wave function by a time-dependent phase and so we define

$$\psi(t) = \Psi(t) \exp \left( -\frac{it}{\hbar} (\bar{E}_0 + 2\bar{L} - 2\bar{J}) \right). \tag{10}$$

Following [15], we also add to the acceptor equation a term of the form  $i \sum_{\ell=1}^3 A_{a,\ell} |\psi_{N-3+\ell}|^2 \psi_{N+1}$ , which describes the transfer of the electron from the  $\alpha$  helix to the acceptor and has a clear physical meaning: The higher the probability of the electron

localization at the terminal end of the helix, the higher the probability of its transfer to the acceptor. It is easy to check that this extra term does not violate conservation of the total electron probability.

From the above Hamiltonian (1) and (7)–(9) one can easily derive the equations for  $U_n$  and  $\Psi_n$ ,

$$\begin{aligned}
i\frac{d\Psi_0}{d\tau} &= (E_d - E_0 - 2L + 2J)\Psi_0 - \sum_{\ell=1}^3 D_{d,\ell}\Psi_\ell + \Psi_0 \sum_{\ell=1}^3 \chi_{d,\ell}(u_\ell - u_0), \\
i\frac{d\Psi_\ell}{d\tau} &= (2J - 2L)\Psi_\ell - J\Psi_{\ell+3} + L[\Psi_{\ell+1} + \Psi_{\ell-1}(1 - \delta_{\ell,1})] - D_{d,\ell}\Psi_0 \\
&\quad + \chi_{d,\ell}\Psi_\ell(u_\ell - u_0) + \chi\Psi_\ell(u_{\ell+3} - u_\ell), \quad \ell = 1, 2, 3, \\
i\frac{d\Psi_n}{d\tau} &= (2J - 2L)\Psi_n - J(\Psi_{n+3} + \Psi_{n-3}) + L(\Psi_{n+1} + \Psi_{n-1}) + \chi\Psi_n(u_{n+3} - u_{n-3}), \quad n = 4, \dots, N-3, \\
i\frac{d\Psi_{N-3+\ell}}{d\tau} &= (2J - 2L)\Psi_{N-3+\ell} - J\Psi_{N-6+\ell} + L[\Psi_{N-4+\ell} + \Psi_{N-2+\ell}(1 - \delta_{\ell,3})] - D_{a,\ell}\Psi_{N+1} \\
&\quad + \chi_{a,\ell}\Psi_{N-3+\ell}(u_{N+1} - u_{N-3+\ell}) + \chi\Psi_{N-3+\ell}(u_{N-3+\ell} - u_{N-6+\ell}) \\
&\quad - iA_{a,\ell}|\Psi_{N+1}|^2\Psi_{N-3+\ell}, \quad \ell = 1, 2, 3, \\
i\frac{d\Psi_{N+1}}{d\tau} &= (E_a - E_0 + 2J - 2L)\Psi_{N+1} - \sum_{\ell=1}^3 D_{a,\ell}\Psi_{N-3+\ell} + \Psi_{N+1} \sum_{\ell=1}^3 \chi_{a,\ell}(u_{N+1} - u_{N-3+\ell}) + i \sum_{\ell=1}^3 A_{a,\ell}|\Psi_{N-3+\ell}|^2\Psi_{N+1}, \\
\frac{d^2u_0}{d\tau^2} &= K_d \left( \sum_{\ell=1}^3 W_{d,\ell}(u_\ell - u_0) + \sum_{\ell=1}^3 \chi_{d,\ell}(|\Psi_0|^2 + |\Psi_\ell|^2) \right), \\
\frac{d^2u_\ell}{d\tau^2} &= W(u_{\ell+3} - u_\ell) + W_{d,\ell}(u_0 - u_\ell) - \chi_{d,\ell}(|\Psi_0|^2 + |\Psi_\ell|^2) + \chi(|\Psi_\ell|^2 + |\Psi_{\ell+3}|^2), \quad \ell = 1, 2, 3, \\
\frac{d^2u_n}{d\tau^2} &= W(u_{n+3} + u_{n-3} - 2u_n) + \chi(|\Psi_{n+3}|^2 - |\Psi_{n-3}|^2), \quad n = 4, \dots, N-3, \\
\frac{d^2u_{N-3+\ell}}{d\tau^2} &= W(u_{N-6+\ell} - u_{N-3+\ell}) + W_{a,\ell}(u_{N+1} - u_{N-3+\ell}) \\
&\quad + \chi_{a,\ell}(|\Psi_{N+1}|^2 + |\Psi_{N-3+\ell}|^2) - \chi(|\Psi_{N-3+\ell}|^2 + |\Psi_{N-6+\ell}|^2), \quad \ell = 1, 2, 3, \\
\frac{d^2u_{N+1}}{d\tau^2} &= K_a \left( \sum_{\ell=1}^3 W_{a,\ell}(u_{N-3+\ell} - u_{N+1}) - \sum_{\ell=1}^3 \chi_{a,\ell}(|\Psi_{N+1}|^2 + |\Psi_{N-3+\ell}|^2) \right), \tag{11}
\end{aligned}$$

where  $\delta_{i,j}$  is the Kronecker delta function. We now need to select the parameter values that best describe the  $\alpha$  helix.

### Parameter values

For the numerical modeling we need to use some numerical values of the parameters. We recall that, in particular, the parameter values for the polypeptide macromolecules are  $J_{\text{amide I}} = 1.55 \times 10^{-22}$  J  $\approx 10^{-3}$  eV,  $J_e \approx 0.1$ – $0.01$  eV  $\approx 10^{-21}$ – $10^{-20}$  J,  $\chi = 35$ – $62$  pN,  $w = 39$ – $58$  N/m, and  $V_{ac} = (3.6$ – $4.5) \times 10^3$  m/s [10]. The molecular weights of large macromolecules which participate in the electron transport chain in redox processes are 980 ku for NADH-ubiquinone oxidoreductase, 480 ku for cytochrome  $bc_1$  complex, and 420 ku for cytochrome  $c$ - $aa_3$  oxidase. The mass of cyt- $c$  is 12 ku, in which the hem-A group has a molecular weight of 852 u and the hem-B group has 616 u, which are 3–5 times larger than the molecular weight (100–200 u) of amino acids that form macromolecules. Studies of the mitochondrial ET chain show that the electrochemical potential for the transfer of an electron is  $E_{ec} = 1.135$  V [56,57].

For completeness of the study we also summarize the data on the parameter values of other relevant compounds in accordance with the discussion in the Introduction. The molecular weights of many conjugated polymer semiconductors vary in the range 10–176 ku and the hole mobility is  $(4 \times 10^{-4})$ – $(1.6 \times 10^{-3})$  cm<sup>2</sup>/(V s). The ionization potential and electron affinity potential for some donor-acceptor copolymer semiconductor molecules are 2.5–4.5 and 1.5–3.1 eV, respectively [58]. The electrochemical band gap  $E_g^{(el)} = E_{IP} - E_{EA}$  is 1.5 eV for poly(5,7-bis(3-dodecylthiophen-2-yl)thieno[3,4- $b$ ]pyrazine) (BTTP), 1.84 eV for poly(5,7-bis(3-dodecylthiophen-2-yl)thieno[3,4- $b$ ]pyrazine-*alt*-1,4-bis(decyloxy)phenylene) (BTTP-P), and 2.24 eV for poly(5,7-bis(3-dodecylthiophen-2-yl)thieno[3,4- $b$ ]pyrazine-*alt*-9,9-dioctyl-2,7-fluorene) (BTTP-F), which are 0.4–0.6 eV larger than the optically determined ones  $E_g^{(opt)} = 1.1$ – $1.6$  eV. This difference can be explained by the exciton binding energy of conjugated polymers which is thought to be in the range of  $E_{ex} \approx 0.4$ – $1.0$  eV [59,60]. Thienopyrazine-based donor-acceptor copolymers such as BTTP,

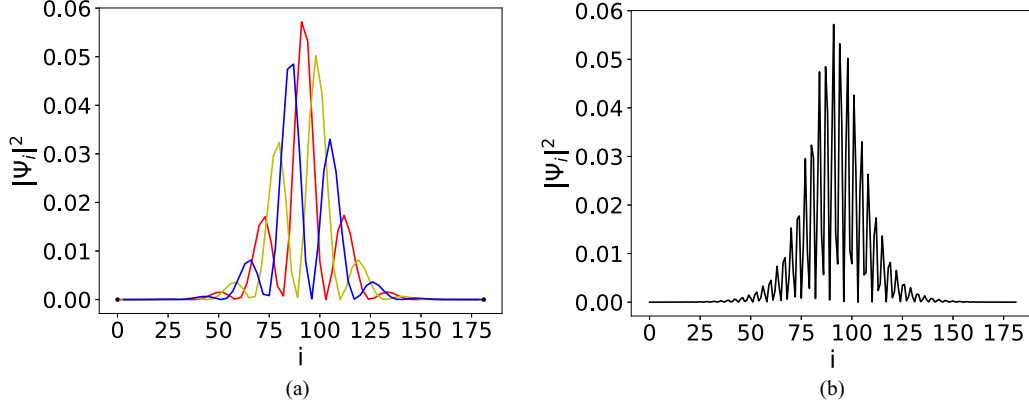


FIG. 2. Polaron with  $E_0 = E_d = E_a = 0$ ,  $J = 0.145$ ,  $L = D_{d,3} = D_{a,1} = 0.231$ ,  $D_{d,1} = D_{d,2} = D_{a,2} = D_{a,3} = 0$ ,  $W = W_{d,1} = W_{d,2} = W_{d,3} = W_{a,3} = 1.825$ ,  $W_{a,1} = W_{a,2} = 0$ ,  $\chi_{d,\ell} = 0.318$ ,  $\chi_{d,\ell} = \chi_{a,\ell} = 0$ ,  $A_{a,\ell} = 0$ , and  $K_d = K_a = 1$ . (a) Electron probability densities are plotted versus the index on the polypeptide chain. Profiles of the three strands are shown as separate curves. (b) Electron density along the  $\alpha$ -helix backbone.

poly(5,7-bis(3-dodecylthiophen-2-yl)thieno[3,4-*b*]pyrazine-*alt*-2,5-thiophene) (BTTP-T), BTTP-F, and BTTP-P have moderate to high molecular weights, broad optical absorption bands that extend into the near-infrared region with absorption maxima at 667–810 nm, and small optical band gaps (1.1–1.6 eV). They show ambipolar redox properties with low ionization potentials [highest occupied molecular orbital (HOMO) levels] of 4.6–5.04 eV. The field-effect mobility of holes varies from  $4.2 \times 10^{-4} \text{ cm}^2/(\text{V s})$  in BTTP-T to  $1.6 \times 10^{-3} \text{ cm}^2/(\text{V s})$  in BTTP-F (see [26]). The reduction potentials of BTTP, BTTP-P, and BTTP-F are  $-1.4$ ,  $-1.73$ , and  $-1.9$  V [vs the saturated calomel electrode (SCE)], respectively. The oxidation potentials of the copolymers are in the range 0.29–0.71 V (vs the SCE). The onset oxidation potential and onset reduction potential of the parent copolymer BTTP are 0.2 and  $-1.3$  V, respectively, which give an estimate for the ionization potential (HOMO level) of 4.6 eV ( $E_{IP} = E_{ox}^{\text{onset}} + 4.4$ ) and an electron affinity (lowest unoccupied molecular orbital level) of 3.1 eV ( $E_{EA} = E_{red}^{\text{onset}} + 4.4$ ). The 4.6-eV  $E_{IP}$  value of BTTP is 0.3 eV lower than that of poly(3-hexylthiophene) (4.9 eV), whereas its  $E_{EA}$  value (3.1 eV) is 0.6 eV higher than that reported for the poly(2,3-dioctylthieno[3,4-*b*]pyrazine) homo-polymer ( $\approx 2.5$  eV). An  $E_{IP}$  value of 4.64 eV and an  $E_{EA}$  value of 2.8 eV were found in the case of BTTP-P [26].

In what follows, we set the on-site electron energy level as the zero of energy, and hence we set  $\bar{E}_0 = 0$ . We are also using a set of model parameters close to those encountered in polypeptide macromolecules or to the bridge-mediated donor-acceptor systems summarized above, i.e.,

$$\begin{aligned} \bar{J} &= 8.42 \times 10^{-23} \text{ J}, & \bar{L} &= 1.34 \times 10^{-22} \text{ J}, \\ \bar{W} &= 10.59 \text{ kg/s}^2, & \bar{\chi} &= 1.85 \times 10^{-11} \text{ J/m}, \end{aligned} \quad (12)$$

corresponding to the following adimensional values of the parameters in our equations:

$$J = 0.145, \quad L = 0.231, \quad W = 1.825, \quad \chi = 0.318. \quad (13)$$

The order of magnitude of these parameters values is close to the parameter values for the electron transport in

polypeptides and for other systems described above. Our aim, for these systems, is to establish a proof of concept of the soliton-mediated long-range ET rather than a performing a detailed study of their actual fine properties.

Before studying the transfer of an electron from the donor to the acceptor we have computed the profile of the static polaron on the helix for the parameters given in (13). This profile is shown in Fig. 2. To obtain this profile, we have relaxed Eqs. (11), using donor-acceptor parameter values so that they do not interact with the chain. One can see clearly from Fig. 2, where the index  $i$  runs along the polypeptide helix and each curve corresponds to a different strand, that the static polaron is a broad localized lump which winds around the polypeptide chain rather than a single soliton located on a single strand or three identical solitons located on each of the strands.

#### IV. CLASSES OF COUPLINGS

Having so far defined a model with a general set of couplings between the  $\alpha$  helix and the donor and acceptor, we will now restrict ourselves to three families of couplings.

In the first set, the donor and the acceptor are coupled to all three strands of the helix using identical coupling parameters. So we have

$$\begin{aligned} D_{d,1} = D_{d,2} = D_{d,3} \neq 0, & \quad D_{a,1} = D_{a,2} = D_{a,3} \neq 0, \\ W_{d,1} = W_{d,2} = W_{d,3} \neq 0, & \quad W_{a,1} = W_{a,2} = W_{a,3} \neq 0. \end{aligned} \quad (14)$$

We call such a configuration the full homogeneous coupling.

The second configuration describes the case in which the donor and the acceptor are coupled to only one strand, so

$$\begin{aligned} D_{d,1} \neq 0, & \quad D_{d,2} = D_{d,3} = 0, \\ D_{a,1} \neq 0, & \quad D_{a,2} = D_{a,3} = 0, \\ W_{d,1} \neq 0, & \quad W_{d,2} = W_{d,3} = 0, \\ W_{a,1} \neq 0, & \quad W_{a,2} = W_{a,3} = 0, \\ A_{a,1} \neq 0, & \quad A_{a,2} = A_{a,3} = 0. \end{aligned} \quad (15)$$

We call this the single-strand coupling. Notice that the donor is coupled to the first peptide of the helix, i.e., to the first

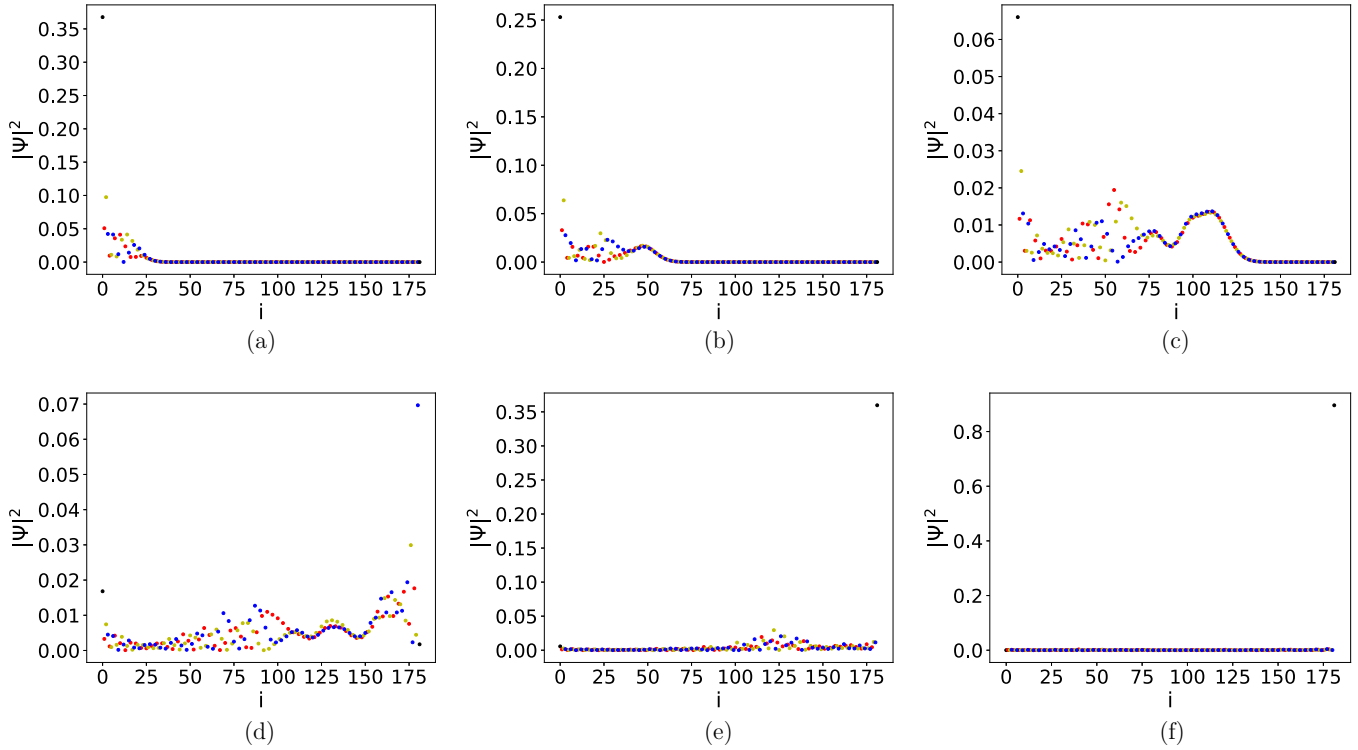


FIG. 3. Profile of  $|\Psi|^2$  for the full homogeneous coupling during the transfer from donor to acceptor for (a)  $\tau = 25$ , (b)  $\tau = 50$ , (c)  $\tau = 100$ , (d)  $\tau = 150$ , (e)  $\tau = 200$ , and (f)  $\tau = 500$ .

peptide group of the first strand, but the acceptor is coupled to the ante-penultimate peptide of the helix, i.e., to the last peptide group on the same strand.

For the third configuration we consider the case when the donor and the acceptor are coupled only to the first and last peptides on the  $\alpha$  helix, so

$$D_{d,1} \neq 0, \quad D_{a,3} \neq 0, \quad W_{d,1} \neq 0, \quad W_{a,3} \neq 0, \quad A_{a,3} \neq 0, \quad (16)$$

while the other parameters are equal to zero. We call this case the end-to-end coupling.

To find the best parameter values for the transfer of the electron from the donor to the acceptor, we have integrated the system of equations (11) numerically on a lattice of 180 PGs. As the initial condition we have set the electron probability

density to 1 on the donor and to 0 everywhere else. We then integrated Eqs. (11) numerically up to  $\tau = 500$ . This time was so chosen because it is roughly 3 times longer than it takes for the polaron to reach the end of the 180-peptide chain. The value of  $|\Psi_{N+1}|^2$  varies with time, but tends to increase modulo some oscillations. To evaluate  $\max |\Psi_{N+1}|^2$  we have tracked its value during the evolution and recorded the largest value obtained before  $\tau \leq 500$ .

We first determined the best donor parameters so that the electron is fully transferred onto the  $\alpha$  helix. We then scanned a very large range of parameter values for the acceptor to determine the one for which the maximum value of the electron probability density on the acceptor,  $\max |\Psi_{N+1}|^2$ , reaches the largest value.

We will now describe the results we have obtained for each type of coupling.

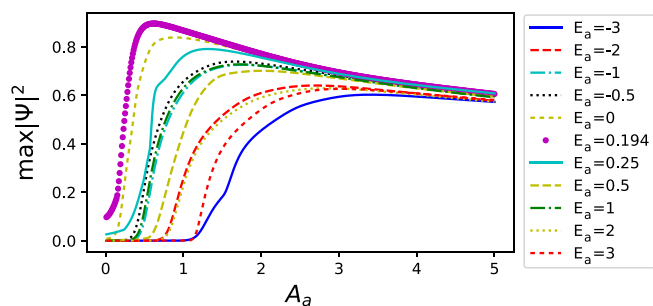


FIG. 4. Full homogeneous coupling: plot of  $\max(|\Psi_{N+1}|^2)$  for  $\tau \leq 500$  as a function of  $A_a$  for different values of  $E_a$  and the parameter values in (14).

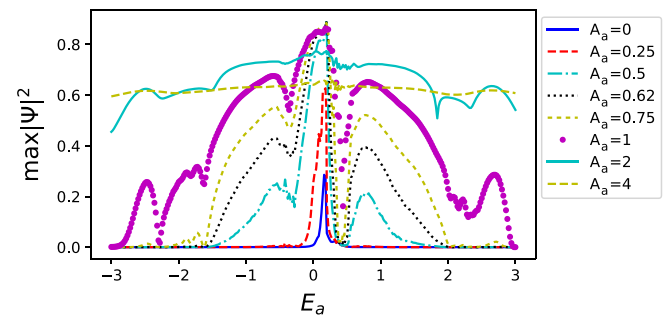


FIG. 5. Full homogeneous coupling: plot of  $\max(|\Psi_{N+1}|^2)$  for  $\tau \leq 500$  as a function of  $E_a$  for different values of  $A_{a,1} = A_{a,2} = A_{a,3} = A_a$  and the parameter values in (14).

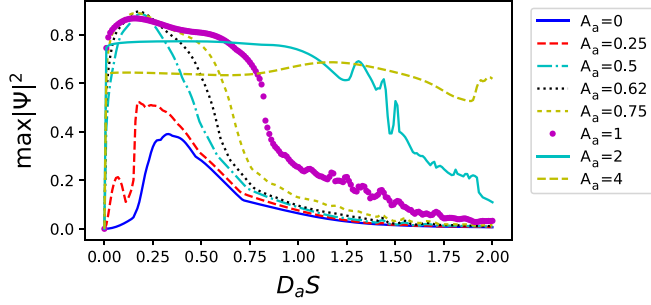


FIG. 6. Full homogeneous coupling: plot of  $\max(|\Psi_{N+1}|^2)$  for  $\tau \leq 500$  as a function of  $D_a S = D_{a,\ell}/J$  for different values of  $A_{a,1} = A_{a,2} = A_{a,3} = A_a$  and the parameter values in (14).

### A. Full homogeneous coupling

The best parameter values we have found to generate a transfer of an electron from the donor to the acceptor are (assuming all the values of  $A_{a,\ell}$ ,  $D_{d,\ell}$ ,  $D_{a,\ell}$ ,  $W_{d,\ell}$ ,  $W_{a,\ell}$ ,  $\chi_{d,\ell}$ , and  $\chi_{a,\ell}$  are the same for  $\ell = 1, 2, 3$ )

$$\begin{aligned} E_d &= 0.25, & D_{d,\ell} &= 0.38J, \\ W_{d,\ell} &= 0.32W, & \chi_{d,\ell} &= 0.62\chi, \\ A_{a,\ell} &= 0.62, & E_a &= 0.194, & D_{a,\ell} &= 0.175J, \\ W_{a,\ell} &= 0.14W, & \chi_{a,\ell} &= 0.27\chi, \end{aligned} \quad (17)$$

and we have found that  $\max|\Psi|^2 = 0.896$  for  $\tau \leq 500$ . In Fig. 3 we present the plots of the time evolution of the electron probability density for the parameters values in (13) and (17). We can see very clearly that the electron is transferred from the donor onto the helix and that it then forms a localized wave that propagates along the helix (see [61]) and has a complex structure. To understand this result, we have to recall the study of soliton formation in  $\alpha$  helices [13] disregarding the donor-acceptor problem. There it was shown that there exist several types of solitons with different energies and symmetries. This comes from the fact that in the energy spectrum of the  $\alpha$  helix there are three peptide groups per elementary cell and so three electron energy bands which correspond to the Davydov splitting. One of these bands is symmetric and has its minimum in the center of the Brillouin zone, at the wave vector  $k = 0$ , while the other two nonsymmetric lower energy bands are degenerate and have their minima at, respectively,  $k_0 = \pm 9\bar{L}/\sqrt{3}(18\bar{J} + \bar{L})$ . As a result, solitons of the first type are formed by the electron from the higher energy band and have an energy which is split from the higher energy band bottom. On the other hand, the solitons of the second type have energies which are split from the degenerate energy band bottoms and are lower than the energy of the first type of soliton. More importantly, there is a hybrid soliton formed by the entanglement (hybridization) of electron probabilities in the two lowest bands due to the Jan-Teller effect and this soliton has the longest lifetime. For the  $\alpha$ -helix parameter values, which we use in our simulations, this hybrid soliton has an energy which is almost 50 times lower than the energy of the first type of soliton. We can expect, and indeed we will see in what follows, that the full homogeneous coupling provides the best conditions for launching the hybrid soliton in the helix as it has the lowest energy and hence leads to the

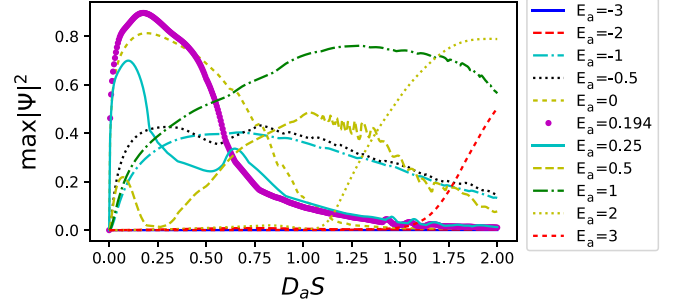


FIG. 7. Full homogeneous coupling: plot of  $\max(|\Psi_{N+1}|^2)$  for  $\tau \leq 500$  as a function of  $D_a S = D_{a,\ell}/J$  for different values of  $E_a$  and the parameter values in (14).

highest probability for the electron to be transported to the opposite end of the helix.

The complex solitonlike wave generated in the helix after the electron has tunneled into it from the donor molecule corresponds, in our numerical simulations, to this hybrid soliton. This hybrid soliton is not localized on a single strand; instead it is distributed between the strands and propagates along the helix with some intrinsic oscillations, rather than along a particular strand, a fact which reflects its hybrid nature. The propagation of this localized polaron is followed by what looks like incoherent ripples. These ripples describe the radiated sound waves in the helix. This is because our system is not completely integrable and while most of the initial electron energy is transferred to the soliton, some of it is converted into oscillating soliton tails.

We then studied how  $\max|\Psi_{N+1}|^2$  varies when the acceptor parameters are varied around their optimal value. This is shown in Figs. 4–9. To perform these simulations, we have defined the parameters

$$D_a S = \frac{D_{a,\ell}}{J}, \quad W_a S = \frac{W_{a,\ell}}{W}, \quad X_a S = \frac{\chi_{a,\ell}}{\chi}, \quad (18)$$

which relate the different parameters of the donor and the acceptor to the corresponding ones on the peptide chain.

From Figs. 4 and 5 we first note that the value of the acceptor electron energy  $E_a$  has to be relatively small for the electron to be transferred to the acceptor and that the values of  $E_a$  and  $A_a$  must be finely tuned for a good “capture” of the electron. The parameters  $D_a$ ,  $W_a$ , and  $\chi_a$ , on the other hand,

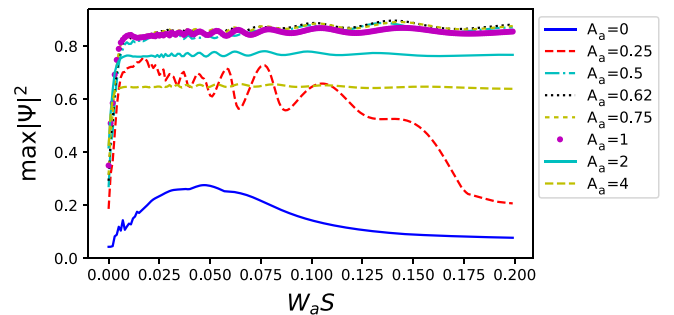


FIG. 8. Full homogeneous coupling: plot of  $\max(|\Psi_{N+1}|^2)$  for  $\tau \leq 500$  as a function of  $W_a S = W_{a,\ell}/W$  for different values of  $A_{a,1} = A_{a,2} = A_{a,3} = A_a$  and the parameter values in (14).

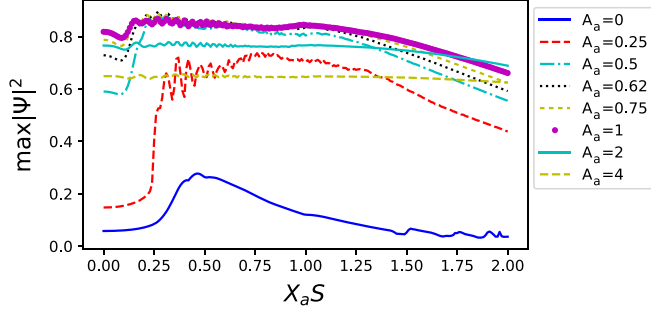


FIG. 9. Full homogeneous coupling: plot of  $\max(|\Psi|^2)$  for  $\tau \leq 500$  as a function of  $\chi_a S = \chi_{a,\ell}/\chi$  for different values of  $A_{a,1} = A_{a,2} = A_{a,3} = A_a$  and the parameter values in (14).

offer a much broader tolerance when  $E_a$  and  $A_a$  are correctly tuned (see Figs. 6–9). This result has a clear physical meaning, since at this last stage of the electron transport the dominant parameters are the strength of the exchange interaction of the acceptor with the helix and the value of the on-site energy level on the acceptor, while, on the other hand, the electron-lattice coupling and the elasticity of the acceptor-helix bond are much less important. Nevertheless, the last stage of the transport process is only possible if a proper soliton has been launched on the helix, carrying most of the initial energy and electron probability to the acceptor with minimal energy dissipation into the lattice vibrations and heat generation.

As we will see in the following sections, the effectiveness of the soliton formation and its parameters are determined by (i) the helix parameters, mainly by the electron-lattice coupling and strand elasticity, and (ii) the number of helix strands coupled to the donor.

### B. Single-strand coupling

In this section we couple the donor only to the first node of the chain:  $D_{d,2} = D_{d,3} = W_{d,2} = W_{d,3} = \chi_{d,2} = \chi_{d,3} = 0$ . We obtain the best transfer from the donor to the chain for the following donor parameters:

$$\begin{aligned} E_d &= 0.25, & D_{d,1} &= 0.38J, \\ W_{d,1} &= 0.32W, & \chi_{d,1} &= 0.62\chi. \end{aligned} \quad (19)$$

Such conditions for the creation of the soliton in the helix are not the optimal ones, since in the soliton formation there

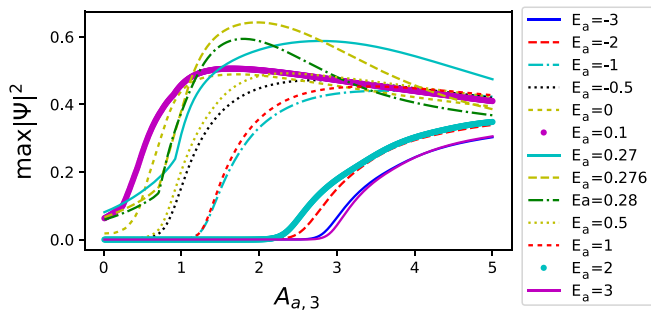


FIG. 10. End-to-end coupling: plot of  $\max|\Psi_{N+1}|^2$  for  $\tau \leq 500$  as a function of  $A_{a,3}$  for different values of  $E_a$  and the parameter values in (18).

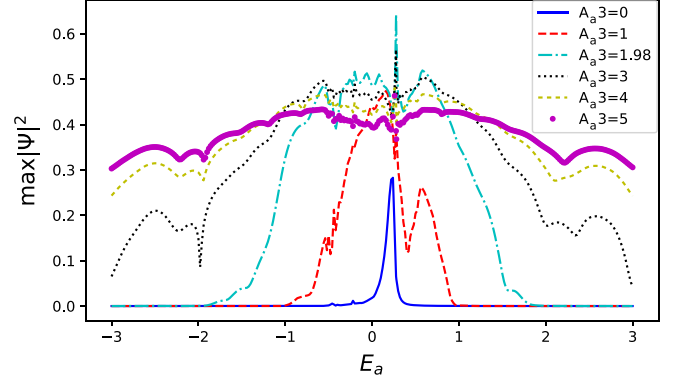


FIG. 11. End-to-end coupling: plot of  $\max|\Psi_{N+1}|^2$  for  $\tau \leq 500$  as a function of  $E_a$  for different values of  $A_{a,3}$  and the parameter values in (18).

will be two contradicting tendencies: redistribution of the electron between the three peptide groups within the same unit cell and its dispersion to the nearest unit cell. These processes will be accompanied by energy dissipation much stronger than in the case of the full homogeneous coupling, and thus will result in the generation of a much weaker soliton i.e., in a less efficient transport of the electron along the helix.

Similarly, the type of coupling between the helix and the acceptor plays an important role in the electron transport, as we will see from this and the next section. First, we consider the coupling of the acceptor to the same strand as the one to which the donor is coupled (single-strand coupling), setting  $A_{a,2} = A_{a,3} = D_{a,2} = D_{a,3} = W_{a,2} = W_{a,3} = \chi_{a,2} = \chi_{a,3} = 0$ .

We have found that the best parameters to obtain a transfer of the electron to the acceptor are

$$\begin{aligned} E_d &= 0.25, & D_{d,1} &= 0.38J, & W_{d,1} &= 0.32W, \\ \chi_{d,1} &= 0.62\chi, & A_{a,1} &= 6.5, & E_a &= 0.265, \\ D_{a,1} &= 0.3J, & W_{a,1} &= 0.37W, & \chi_{a,1} &= \chi. \end{aligned} \quad (20)$$

As one could expect, the maximum value of the electron probability on the acceptor  $|\Psi_{N+1}|^2$  for  $\tau \leq 500$  in this case is much lower than in the full homogeneous case and is equal to only 0.218 39, showing that in this configuration, the electron is transferred to the acceptor with only a 20% probability.

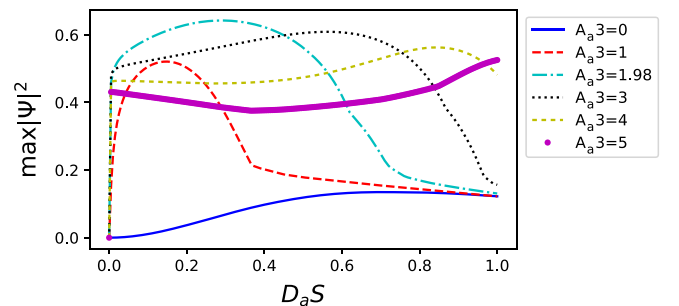


FIG. 12. End-to-end coupling: plot of  $\max|\Psi_{N+1}|^2$  for  $\tau \leq 500$  as a function of  $D_a S = D_{a,\ell}/J$  for different values of  $A_{a,3}$  and the parameter values in (18).

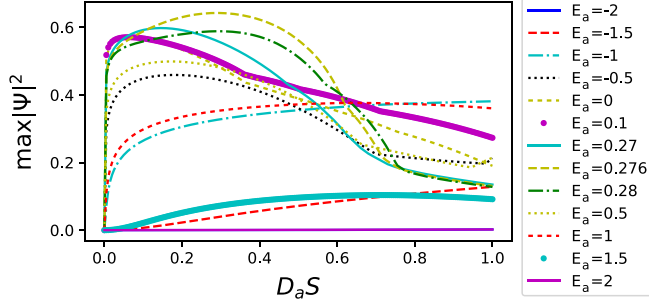


FIG. 13. End-to-end coupling: plot of  $\max |\Psi_{N+1}|^2$  for  $\tau \leq 500$  as a function of  $D_a S = D_{a,\ell}/J$  for different values of  $E_a$  and the parameter values in (18).

As this is quite small, we did not study the variation of  $\max |\Psi_{N+1}|^2$  around these optimal values of the parameters.

### C. End-to-end coupling

To couple the acceptor to the last peptide of the helix, we set  $A_{a,1} = A_{a,2} = D_{a,1} = D_{a,2} = W_{a,1} = W_{a,2} = \chi_{a,1} = \chi_{a,2} = 0$ . In this case we have obtained the best transfer using the parameters

$$\begin{aligned} E_d &= 0.25, & D_{d,1} &= 0.38J, & W_{d,1} &= 0.32W, \\ \chi_{d,1} &= 0.62\chi, & A_{a,3} &= 1.98, & E_a &= 0.276, \\ D_{a,3} &= 0.29J, & W_{a,3} &= 0.002W, & \chi_{a,3} &= 0.04\chi, \end{aligned} \quad (21)$$

and with this choice we have found that  $\max |\Psi_{N+1}|^2 = 0.642558$ , which is higher than in the previous case, although lower than in the case of the full homogeneous coupling.

We then studied how  $\max |\Psi_{N+1}|^2$  varies when the acceptor parameters are varied around their optimal value. This is shown in Figs. 10–15. As with the full homogeneous coupling, we have found that the absorption is mainly controlled by a fine-tuning between  $A_{a,3}$  and  $E_a$  but that there is a broader tolerance for the values of  $D_a$ ,  $W_a$ , and  $\chi_a$ .

Having analyzed the parameter stability of our model, we now turn to the study of its thermal stability.

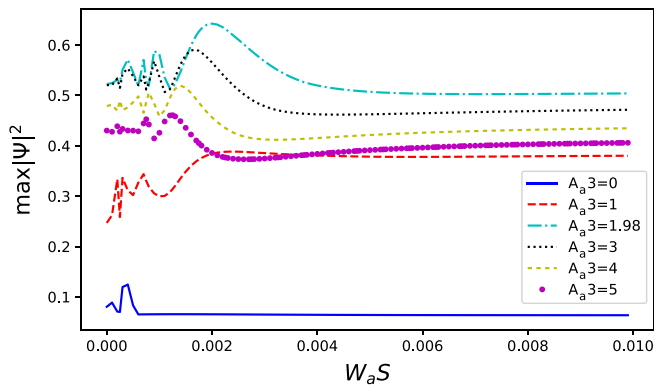


FIG. 14. End-to-end coupling: plot of  $\max |\Psi_{N+1}|^2$  for  $\tau \leq 500$  as a function of  $W_a S = W_{a,\ell}/W$  for different values of  $A_{a,3}$  and the parameter values in (18).

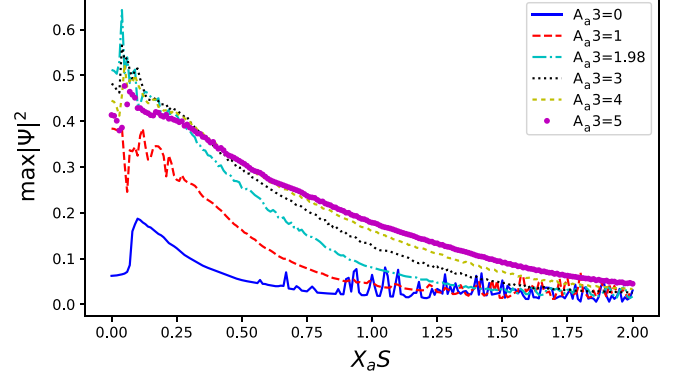


FIG. 15. End-to-end coupling: plot of  $\max |\Psi_{N+1}|^2$  for  $\tau \leq 500$  as a function of  $\chi_a S = \chi_{a,\ell}/\chi$  for different values of  $A_{a,3}$  and the parameter values in (18).

### V. THERMAL STABILITY OF THE SOLITON-MEDIATED ELECTRON TRANSPORT

So far in the study of our model, we have not taken into account any thermal fluctuations. To include them we have modified the model by adding to the equations for  $U_n$  the Langevin terms

$$L_n = F_n(\tau) - \Gamma \frac{du_n}{d\tau}, \quad (22)$$

where  $\Gamma$  is an absorption parameter and  $F_n(\tau)$  represents the thermal noise modeled as a Gaussian white noise of zero mean value and variance given by

$$\langle F_n(\tau_1) F_m(\tau_2) \rangle = 2\Gamma kT \delta(\tau_1 - \tau_2) \delta_{n,m}, \quad (23)$$

where  $k$  is the Boltzmann coefficient and for the dimensional thermal energy  $kT$  we have  $kT = k\bar{T}/\hbar v$ . To implement this numerically,  $F(\tau)$  has to be kept constant during each time step  $d\tau$  and so we have used  $\delta(\tau_1 - \tau_2) = 1/d\tau$ .

For each temperature, we have performed 100 simulations and computed the mean values of  $\max |\Psi_a|$ , for  $\tau \leq 100$ , obtained from these simulations. At physiological

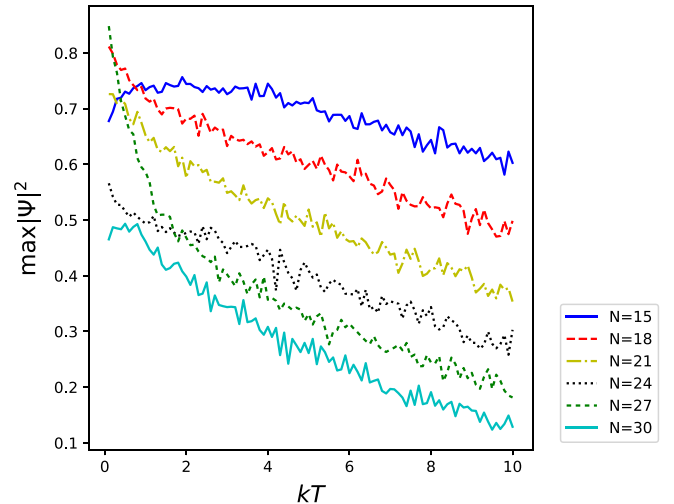


FIG. 16. Full homogeneous coupling: plot of  $\max |\Psi_{N+1}|^2$  for  $\tau \leq 100$  as a function of  $kT$  for different values of the chain length  $N$  and  $\Gamma = 0.2$ .

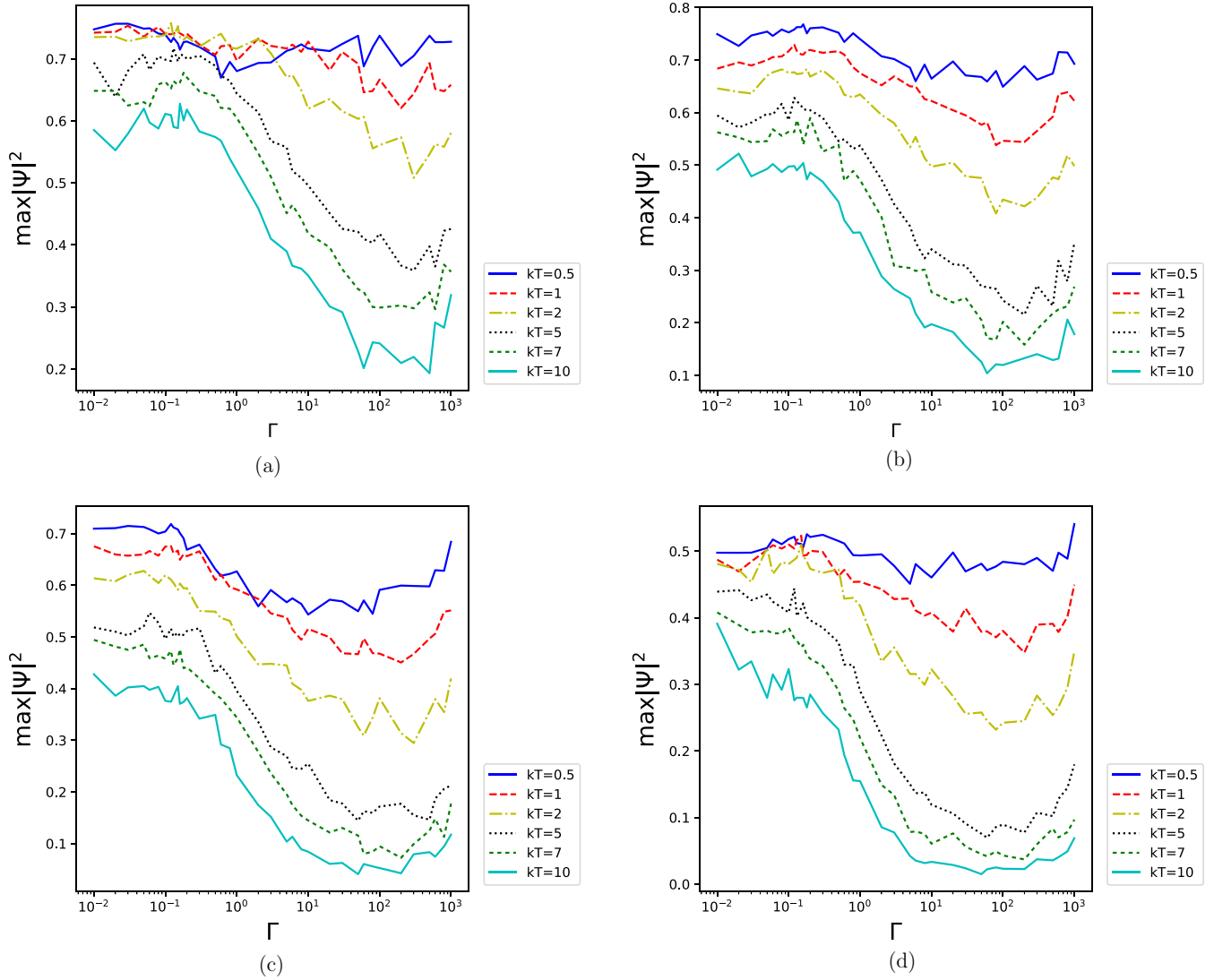


FIG. 17. Full homogeneous coupling: plot of  $\max |\Psi_{N+1}|^2$  for  $\tau \leq 500$  as a function of  $\Gamma$  for different values of  $kT$  and (a)  $N = 15$ , (b)  $N = 18$ , (c)  $N = 21$ , and (d)  $N = 24$ .

temperature,  $\overline{kT} \approx 0.025$  eV, which in our adimensional units corresponds to 7.12. We have thus varied  $kT$  between 0 and 10 to capture the physiological conditions when  $\overline{J}$  is smaller than 0.035 eV.

In Fig. 16 we present the variation of  $\max |\Psi_{N+1}|^2$  as a function of temperature for different chain lengths. We see that for short chains the temperature has a minimal effect, while for longer chains its influence is more pronounced.

It is worth recalling that although large proteins in electron transport chains can consist of up to a few thousand amino acids, the  $\alpha$ -helical parts of their globular structure consist of up to  $N = 50$ –70 peptide groups. In transmembrane proteins the  $\alpha$  helices are even shorter, with  $N = 30$  or even smaller. Moreover, in the biggest enzymes of an electron transport chain, such as NADH ubiquinone oxidoreductase, which is the first and the biggest protein complex of the respiratory chain, there is a whole pathway for the electron transport prior to the ubiquinone reduction via several iron sulfur clusters, connected by relatively short  $\alpha$  helices (see [8]). So we conclude that under physiological conditions, the transfer

of the electron from a donor to an acceptor is thermally stable.

Looking at the data in Fig. 17, we see that the probability of an electron transfer from the donor to the acceptor is relatively constant when  $\Gamma < 1$  and so it does not play a significant role in the thermal stability of the electron transfer. In [15],  $\Gamma$ , which can only be estimated, was taken to be 0.2.

## VI. CONCLUSION

In this paper we have presented a model describing the long-range transport of an electron from a donor molecule to an acceptor one via the nonlinear state of a large polaron (solitonlike state) formed in a  $\alpha$ -helical protein in a donor- $\alpha$ -helix-acceptor system. Conventionally, we model the  $\alpha$  helix as a polypeptide chain, twisted in a helix, in which each peptide group is coupled to its nearest neighbors by a chemical bond and to every third neighbor by a hydrogen bond. The helix can thus be described as three parallel strands coupled to each other. We have found that the static polaron on such a

helix, for the parameters that describe amide I vibration in a  $\alpha$ -helical protein, is a relatively broad localized hump extended over the polypeptide macromolecule, in agreement with other studies (see, e.g., [11,13]). In our model we have only taken into account one phonon mode, while in real proteins there are many other phonon modes, the interaction with which results in a bigger value of the effective electron-lattice coupling, and hence in stronger soliton localization than obtained here.

We then studied the transfer of an electron from a donor molecule to the acceptor by initially placing the electron on the donor. For the proper parameters of the couplings, the electron was, within a very short time interval, transferred onto the polypeptide chain, where it was self-trapped in a polaron state, and then moved towards the other extremity of the chain where it was absorbed by the acceptor.

We have considered three types of couplings between the donor and the polypeptide chain as well as between the acceptor and the polypeptide chain. In the first case, the donor and the acceptor were coupled, respectively, to the first three and the last three nodes of the chain, using identical parameters, and we called such a configuration the fully homogeneous one. In the second configuration, the donor was coupled to the first node of the chain and the acceptor to the last node of the same strand or to the last node of the helix. We call such couplings single-strand and end-to-end couplings, respectively.

The fully homogeneous coupling is the one that leads to the best donor-acceptor electron transport with an efficiency of 90% or more depending on the length of the chain. The end-to-end coupling did not work so well but still led to a transfer probability of up to 60%, while the single-strand one was the worst, leading only to a 20% probability transfer. These results can be explained from the dependence of the efficiency of the soliton generation not only on the actual parameter values of the system but also on the type of couplings between the helix, the donor, and the acceptor. If one uses the inverse scattering theory for integrable systems, applied to the time evolution of certain initial conditions for the nonlinear Schrödinger equation that approximates Davydov solitons [16,17], these different couplings translate into specific initial conditions which lead to families of solitons with different efficiencies.

Our study has shown that an electron in the polaron (solitonlike) state can easily propagate as a traveling wave along the  $\alpha$ -helical chain. The polaron that is generated in the helix in the vicinity of the donor molecule has a complex internal structure: It is not just a clean simple polaron localized on a single strand; instead, it is distributed between the strands and propagates along the helix with some intrinsic oscilla-

tions, rather than along a particular strand, which reflects its collective hybrid nature.

Unfortunately, the exact value of the exchange interaction for an extra electron in proteins is not known, but can be roughly estimated at 0.05–0.1 eV, comparable to  $\bar{J}$ , and the other parameters are the same as for amide I vibration, which were used in our model. Other related manufactured donor- $\alpha$ -helix-acceptor systems, described in the Introduction, have parameter values close to those considered here, so we can conclude that our model for the long-range electron transport describes these systems as well. Our results explain the experimental evidence that the donor and acceptor parameters, as well as the type of their coupling, affect the electron transport in donor- $\alpha$ -helix-acceptor systems (see [62,63]).

We have also shown that when we add thermal fluctuations to the model, the long-range electron transfer in the donor- $\alpha$ -helix-acceptor system is stable at physiological temperatures. We have thermalized a mixed quantum classical system in a way which makes the quantum part behave classically as well. According to [64], this results in a broadening of the soliton wave function in the helix and in a decrease of the binding energy of the soliton. This in turn results in a lower stability of the soliton with respect to any perturbation, including thermal fluctuations, compared to a proper analysis of the thermal stability. Moreover, as shown in [65], accounting for temperature fluctuations in the equation for lattice displacements within a quantum-mechanical description results in an effective decrease of the resonant interaction energy by the exponential Debye-Waller factor. This then leads to a decrease of the spatial dispersion of the electron and an increase of the electron-lattice coupling, which itself results in an increase of the binding energy of the soliton and, as a result, a higher thermal stability compared to our model. A proper analysis of thermal stability of electron transport would require a more rigorous treatment and could be the topic of a paper on its own. In this paper we have decided to restrict ourselves to the simplest analysis.

#### ACKNOWLEDGMENTS

L.S.B. acknowledges partial support from Budget Program No. KPKVK 6541230 and Scientific Program No. 0117U00236 of the Department of Physics and Astronomy of the National Academy of Sciences of Ukraine and thanks the Department of Mathematical Sciences of the University of Durham for hospitality during her short-term visit. W.J.Z. thanks the Leverhulme Trust for support through Grant No. EM-2016-007.

- 
- [1] *Electron Transfer: From Isolated Molecules to Biomolecules*, edited by J. Jortner and M. Bixon (Wiley, New York, 1999), Vol. 106.
- [2] D. Voet and J. G. Voet, *Biochemistry*, 3rd ed. (Wiley, New York, 2004).
- [3] T. Förster, *Ann. Phys. (Leipzig)* **437**, 55 (1948).
- [4] M. Kasha, in *Physical and Chemical Mechanisms in Molecular Radiation Biology*, edited by W. A. Glass and M. N. Varma, Basic Life Sciences Vol. 58 (Springer, New York, 1992), pp. 231–255.
- [5] G. A. Jones and D. S. Bradshaw, *Front. Phys.* **7**, 100 (2019).
- [6] R. K. Murray, D. K. Granner, P. A. Mayes, and V. W. Rodwell, *Harper's Illustrated Biochemistry* (McGraw-Hill, New York, 2003), p. 96.
- [7] T. Althoff, D. J. Mills, J.-L. Popot, and W. Khlbrandt, *EMBO J.* **30**, 4652 (2011).
- [8] A. S. Davydov and N. I. Kislukha, *Physica Status Solidi B* **59**, 465 (1973).
- [9] A. S. Davydov, *Solitons in Molecular Systems* (Reidel, Dordrecht, 1985).

- [10] A. C. Scott, *Phys. Rep.* **217**, 1 (1992).
- [11] A. S. Davydov, A. A. Eremko, and A. I. Sergienko, *Ukr. J. Phys.* **23**, 983 (1978).
- [12] V. K. Fedyanin and L. V. Yakushevich, *Int. J. Quantum Chem.* **21**, 1019 (1982).
- [13] L. Brizhik, A. Eremko, B. Piette, and W. Zakrzewski, *Phys. Rev. E* **70**, 031914 (2004).
- [14] L. S. Brizhik and A. A. Eremko, *Z. Phys. B* **104**, 771 (1997).
- [15] L. S. Brizhik, B. M. A. G. Piette, and W. J. Zakrzewski, *Phys. Rev. E* **90**, 052915 (2014).
- [16] L. S. Brizhik and A. S. Davydov, *Phys. Status Solidi B* **115**, 615 (1983).
- [17] L. S. Brizhik, *Phys. Rev. B* **48**, 3142 (1993).
- [18] D. G. Nicholls and S. J. Ferguson, *Bioenergetics 3* (Academic, New York, 2002).
- [19] C. W. F. McClare, *Ann. NY Acad. Sci.* **227**, 74 (1974).
- [20] N. A. Nevskaya and Y. N. Chirgadze, *Biopolymers* **15**, 639 (1976).
- [21] A. S. Davydov, *Biology and Quantum Mechanics (Monographs in Natural Philosophy)*, 1st ed., International Series in Natural Philosophy Vol. 109 (Pergamon, Oxford, 1981).
- [22] G. Careri, in *Cooperative Phenomenon*, edited by H. Haken and W. Wagner (Springer, Berlin, 1973), pp. 391–394.
- [23] Z. Ganim, H. S. Chung, A. W. Smith, L. P. Deflores, K. C. Jones, and A. Tokmakoff, *Acc. Chem. Res.* **41**, 432 (2008).
- [24] *Spectroscopy of Biological Molecules: Proceedings from the 14th European Conference on the Spectroscopy of Biological Molecules 2011*, edited by M. P. Marques, L. A. E. Batista de Carvalho, and P. I. Haris (IOS, Amsterdam, 2013).
- [25] J. A. Roberts, J. P. Kirby, and D. G. Nocera, *J. Am. Chem. Soc.* **117**, 8051 (1995).
- [26] Y. Zhu, R. D. Champion, and S. A. Jenekhe, *Macromolecules* **39**, 8712 (2006).
- [27] D. Li, C. Sun, H. Li, H. Shi *et al.*, *Chem. Sci.* **8**, 4587 (2017).
- [28] Q. Van Nguyen, P. Martin, D. Frath, M. L. Della Rocca, F. Lafolet, S. Bellinck, P. Lafarge, and J.-C. Lacroix, *J. Am. Chem. Soc.* **140**, 10131 (2018).
- [29] L. Tian, Z. Hu, X. Liu, Z. Liu, P. Guo, B. Xu, Q. Xue, H.-L. Yip, F. Huang, and Y. Cao, *ACS Appl. Mater. Interfaces* **11**, 5289 (2019).
- [30] H. Li, F. S. Kim, G. Ren, and S. A. Jenekhe, *J. Am. Chem. Soc.* **135**, 14920 (2013).
- [31] H. A. M. van Mullekom, J. A. J. M. Vekemans, E. E. Havinga, and E. W. Meijer, *Mater. Sci. Eng.* **32**, 1 (2001).
- [32] Y. Garcia-Basabe, G. Kladnik, C. F. N. Marchiori, C. E. V. de Moura, L. Floreano, A. B. Rocha, L. S. Roman, A. Morgante, D. Cvetko, and M. L. M. Rocco, *J. Phys. Chem. C* **121**, 25187 (2017).
- [33] G. Yu, J. Gao, J. C. Hummelen, F. Wudl, and A. J. Heeger, *Science* **270**, 1789 (1995).
- [34] L. M. Campos, A. Tontcheva, S. Günes, G. Sonmez, Neugebauer, N. S. Sariciftci, and F. Wudl, *Chem. Mater.* **17**, 4031 (2005).
- [35] M. Svensson, F. Zhang, S. C. Veenstra, W. J. H. Verhees, C. Hummelen, J. M. Kroon, O. Inganas, and M. R. Andersson, *Adv. Mater.* **15**, 988 (2003).
- [36] S. Admassie, O. Inganas, W. Mammo, E. Perzon, and M. R. Andersson, *Synth. Met.* **156**, 614 (2006).
- [37] A. P. Kulkarni, Y. Zhu, and S. A. Jenekhe, *Macromolecules* **38**, 1553 (2005).
- [38] C. Ego, D. Marsitzky, S. Becker, J. Zhang, A. C. Grimsdale, Mullen, J. D. MacKenzie, C. Silva, and R. H. Friend, *J. Am. Chem. Soc.* **125**, 437 (2003).
- [39] B. C. Thompson, L. G. Madrigal, M. R. Pinto, T.-S. Kang, K. S. Schanze, J. R. Reynolds, *J. Polym. Sci. A* **43**, 1417 (2005).
- [40] W.-C. Wu, C.-L. Liu, and W.-C. Chen, *Polymer* **47**, 527 (2006).
- [41] A. Babel, J. D. Wind, and S. A. Jenekhe, *Adv. Funct. Mater.* **14**, 891 (2004).
- [42] T. Yamamoto, T. Yasuda, Y. Sakai, and S. Aramaki, *Macromol. Rapid Commun.* **26**, 1214 (2005).
- [43] T. Yasuda, Y. Sakai, S. Aramaki, and T. Yamamoto, *Chem. Mater.* **17**, 6060 (2005).
- [44] S. Chen, K. C. Lee, Z.-G. Zhang, D. S. Kim, Y. Li, and C. Yang, *Macromolecules* **49**, 527 (2016).
- [45] H. Zhang, S. Zhang, Y. Mao, K. Liu, Y.-M. Chen, Z. Jiang, J. Strzalka, W. Yang, C.-L. Wang, and Y. Zhu, *Polym. Chem.* **8**, 3255 (2017).
- [46] M. Chen, X. Crispin, E. Perzon, M. R. Andersson, T. Pullerits, M. Andersson, O. Inganas, and M. Berggren, *Appl. Phys. Lett.* **87**, 252105 (2005).
- [47] L. Sepunaru, S. Refaely-Abramson, R. Lovrinčić, Y. Gavrilo, P. Agrawal, Y. Levy, L. Kronik, I. Pecht, M. Sheves, and D. Cahen, *J. Am. Chem. Soc.* **137**, 9617 (2015).
- [48] P. G. M. Mileo, K. Adil, L. Davis, A. Cadiou, Y. Belmabkhout, H. Aggarwal, G. Maurin, M. Eddaoudi, and S. Devautour-Vinot, *J. Am. Chem. Soc.* **140**, 13156 (2018).
- [49] N. L. Ing, M. Y. El-Naggar, and A. I. Hochbaum, *J. Phys. Chem. B* **122**, 10403 (2018).
- [50] N. Amdursky, *Phys. Chem. Chem. Phys.* **15**, 13479 (2013).
- [51] S. Xu, A. Barrozo, L. M. Tender, L. M. Tender, A. I. Krylov, and M. Y. El-Naggar, *J. Am. Chem. Soc.* **140**, 10085 (2018).
- [52] S. K. M. Nalluri, C. Berdugo, N. Javid, P. W. J. M. Frederix, and R. V. Ulijn, *Angew. Chem. Int. Ed.* **53**, 5882 (2014).
- [53] Y. Tan, R. Y. Adhikari, N. S. Malvankar, S. Pi, J. E. Ward, T. L. Woodard, K. P. Nevin, Q. Xia, M. T. Tuominen, and D. R. Lovley, *Small* **12**, 4481 (2016).
- [54] B. Akdim, R. Pachter, and R. R. Naik, *Appl. Phys. Lett.* **106**, 183707 (2015).
- [55] A. S. Davydov and A. D. Suprun, *Ukr. J. Phys.* **19**, 44 (1974).
- [56] G. S. Engel, T. R. Calhoun, E. L. Read, T. K. Ahn, T. Mancal, Y. C. Cheng, R. E. Blankenship, and G. R. Fleming, *Nature (London)* **446**, 782 (2007).
- [57] E. Collini, C. Y. Wong, K. E. Wilk, P. M. G. Curmi, P. Brumer, and G. D. Scholes, *Nature (London)* **463**, 644 (2010).
- [58] T. Renger, V. May, and O. Kühn, *Phys. Rep.* **343**, 137 (2001).
- [59] H. Wang, S. Lin, J. P. Allen, J. C. Williams, S. Blankert, C. Laser, and N. W. Woodbury, *Science* **316**, 747 (2007).
- [60] D. J. Voet, J. G. Voet, and C. W. Pratt, *Principles of Biochemistry*, 3rd ed. (Wiley, London, 2008), Chap. 18, p. 608.
- [61] See Supplemental Material at <http://link.aps.org/supplemental/10.1103/PhysRevE.100.062205> for a movie.
- [62] X. U. Jiang, K. Ataka, and J. Heberle, *J. Phys. Chem. C* **112**, 813 (2008).
- [63] H. Guo, T. Kimura, and Y. Furutani, *Chem. Phys.* **419**, 8 (2013).
- [64] L. Cruzeiro-Hansson and S. Takeno, *Phys. Rev. E* **56**, 894 (1997).
- [65] L. S. Brizhik, A. S. Davydov, and I. M. Pershko, *Theor. Math. Phys.* **77**, 1129 (1988).